Research Article

Ge Gao, Qiang Li, Hongjie Luo* and Xiao Huang*

Effect of particle size distribution on microstructure and chloride permeability of blended cement with supplementary cementitious materials

https://doi.org/10.1515/secm-2022-0226
received May 25, 2023; accepted September 11, 2023

Abstract: In order to improve the chloride ion penetration resistance of supplementary cementitious materials (SCMs) in blended cement, this study optimizes the particle size distribution of cementitious components based on the Fuller model. Portland cement (PC), fly ash (FA), and ground granulated blast furnace slag (GGBFS) are successfully divided into four particle size ranges by precision air classifier, which are 0–8, 8–30, 30–50, and 50–80 μm, respectively. The optimum cementitious materials in four ranges based on 28-day compressive strength are determined by nine groups of orthogonal tests. The blended cement with optimal performance is obtained by GGBFS in 0–8 μm, PC in 8–30 μm, GGBFS in 30–50 μm, and FA in 50–80 μm. The results show that the blended cement with SCMs based on Fuller model have superior microstructure and chloride ion penetration resistance, which is due to their smaller pore size, a strong volcanic ash effect, and chloride ion binding ability. In addition, this research presents a novel approach for realizing the application of a large amount of SCMs in blended cement.

Keywords: supplementary cementitious materials, particle size distribution, chloride diffusion coefficient

*** Corresponding author: Hongjie Luo,** Institute for the Conservation of Cultural Heritage, Shanghai University, Shanghai 200444, China, e-mail: hongjieluo@shu.edu.cn
*** Corresponding author: Xiao Huang,** Institute for the Conservation of Cultural Heritage, Shanghai University, Shanghai 200444, China, e-mail: xhuang@shu.edu.cn
Ge Gao: School of Materials Science and Engineering, Shanghai University, Shanghai 200444, China; Institute for the Conservation of Cultural Heritage, Shanghai University, Shanghai 200444, China
Qiang Li: School of Materials Science and Engineering, Shanghai University, Shanghai 200444, China; Institute for the Conservation of Cultural Heritage, Shanghai University, Shanghai 200444, China; Ancient Ceramics Research Center, Shanghai Institute of Ceramics Chinese Academy of Sciences, Shanghai 200050, China

1 Introduction

Concrete is the most essential building material in the world, and Portland cement (PC) is an indispensable cementitious material in the production of concrete [1,2]. However, the production of cement produces large amounts of polluting gases (SO_2, CO_2, and NO_x) and dust, which have an enormous impact on the environment [3–5]. In addition, the production of cement consumes large amounts of nonrenewable resources such as clay, limestone, and coal [6]. In order to solve such problems in cement-based materials, supplementary cementitious materials (SCMs) such as fly ash (FA), granulated slag, and silica fume can be partially used to replace cement, which expands the application range and field of cement concrete [7].

The effects of SCMs on cement-based materials can be classified as inherent characteristic effect, particle size refinement effect, and hydration effect [8,9]. As a mineral admixture with a pozzolanic effect, FA has an essential function in cement paste compatibility and is extensively applied in cementitious materials [10]. The shape of FA particles is spherical with a smooth and dense surface, which has a water-reducing effect [11]. The hydration reaction of FA is relatively slow at room temperature, and its active components SiO_2 and Al_2O_3 react with the silicon hydroxide produced by the hydration reaction of cement to produce hydrated C–S(Al)–H gel, which then reacts with $CaSO_4$ to produce calcium alumina or monosulfide type calcium sulfur aluminate [12–14]. The hydration reaction of FA inhibits the alkali aggregate reaction and proceeds mainly in the pores of cement paste [15]. It reduces the porosity inside the concrete, increases the compactness of the concrete, improves the interface area between the aggregates and the cement paste, and promotes the growth of the strength of the concrete at a later stage [16]. GGBFS is a granulated vitreous material with potential hydration activity that has been widely applied in the cement and

concrete industries [17,18]. By adding the appropriate amount of mineral powder to the cementitious material, it can provide the cementitious material with excellent compatibility, high durability, various excellent mechanical properties, volume stability, and economic rationality.

The particle size distribution (PSD) of cementitious materials has an important influence on the heat evolution, microstructure, and mechanical properties of cementitious materials [19,20]. The rheological and mechanical properties of cement are closely related to its PSD [21]. In order to achieve better performance of composite cement paste, most research studies employ PSD model to modify the reasonable PSD of cementitious material system [22]. Fine particles are able to fill the voids between large particles and increase the packing density by reducing the volume, which has a positive effect on their flow, mechanical, and rheological properties [23]. FA below 45 μm has a contribution to the compressive strength of blended cement, which is mainly due to the fine FA particles promoting the hydration reaction, Ca^{2+}, Na^{+}, and K^{+} concentration decreases with the decrease of particle size [24]. The PSD of FA affects its activity, which in consequence determines the crystallization nucleation process occurring at the particle interface [25]. The calcium–silica ratio directly affects the reactivity of the slag particles, which have a higher CaO and Al_2O_3 content in the fine particle range and consequently a higher hydration degree [26]. GGBFS particles below 30 μm hydrate up to 60% at 24 h; therefore, particle size has a large effect on the exothermic heat of hydration [27]. Consequently, the use of SCMs combined with particle distribution has great potential to improve the various performances of blended cements.

In coastal areas, 89% of concrete bridges serving 7–25 years have chloride erosion problems [28]. Chloride ion erosion destroys the passivation film on the surface of steel reinforcement and endangers the structural safety of marine concrete [29]. Chlorine ions from seawater penetrate the steel reinforcement in the concrete, causing continuous rusting of the reinforcement and thus internal stresses, leading to cracking and spalling of the concrete [30]. In order to improve the chloride ion penetration resistance of composite cement mortar and reduce energy consumption, most research have incorporated SCMs into cement [31]. It has been found that the higher the slag content in the cement paste, the denser cement matrix hinders the penetration of chloride ions, and thus the lowers the penetration depth [32]. The reduction in slag content produces more N–A–S–H gels and fewer C–(A)–S–H gels, resulting in increased penetration of chloride ions [33]. Chloride ions can be adsorbed on the surface of C–S–H gels to undergo physical binding. The degree of binding of chloride ions in C–S–H is determined by the calcium to silicon ratio, and the lower the ratio the lower the binding capacity [34].

It is necessary to optimize the particle distribution of SCMs in order to improve the chloride ion penetration resistance of the composite cement paste. In Section 2, the cementitious materials were divided into four particle size ranges, the nine groups of orthogonal tests of 28-day compressive strength in each particle size range of cementitious materials were designed, and the optimum cementitious materials in four ranges based on the Fuller distribution model were determined. In Section 3, the compressive strength, hydration properties, and chloride ion penetration resistance of the blended cement were investigated and analyzed. This research presents a novel approach for realizing the application of a large amount of SCMs in blended cement.

2 Experimental

In this section, the preparation of raw materials, the specific steps of the test methods, and the design of orthogonal tests are presented.

2.1 Raw materials

P.I 42.5 PC, class I FA (FA), and S95 ground granulated blast furnace slag (GGBFS) conforming to Chinese National Standards GB175-2007, GB/T1596-2005, and GB/T18046-2008, respectively, were used as cementitious materials in this study. The PSD of raw materials is shown in Figure 1.

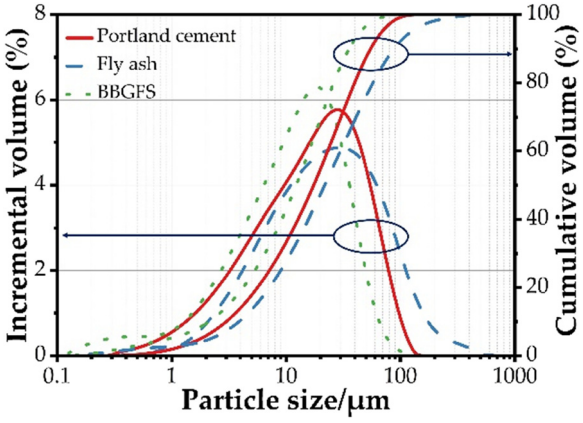

Figure 1: PSD of PC, FA, and GGBFS.

2.2 Samples preparation and characterization

The cementitious materials with different particle size ranges (0–8, 8–3, 30–50, 50–80 μm) were obtained by precision air classifier (LNPE Power Equipment Co., Ltd). The PSD of these is shown in Figure 2. The particle morphology of cementitious materials with different particle size ranges is shown in Figures S2–S4. The PSD of these was determined by the laser particle size analyzer (Mastersizer3000). The water to binder ratio (W/B) of the blended pastes was 0.4 and the paste samples were cast into 20 × 20 × 20 mm^3 molds (A W/B ratio of 0.40 is suggested in ASTM C1608 [35]). After being cured at 20 ± 1°C and a relative humidity of 90% for 24 h, the sample were demolded and cured in lime saturated water to testing ages, followed by the strength tests according to EN 196-1 [36]. The hydration evolution of blended cement pastes was measured by isothermal calorimeter (TAM air, TA, American) at 20°C within 72 h according to ASTM C1702-09A [37]. Hydration products of blended cement pastes were measured by thermogravimetry (Mettler Toledo TGA/DSC 3), approximately 15 mg of sample was heated in a N_2-gas flowing atmosphere with temperature increase at rate of 10°C/min from 20 to 1,000°C. The pore structure of blended cement paste was measured by MIP measurements (Micrometrics PoroSizer 9320), and the measured pore size is in the range from 0.007 to 400 mm. The microscopic morphology of blended cement pastes was observed by using scanning electron microscope (Mwelin Compact, Carl Zeiss NTS GmbH, German). The W/B ratio and cement–sand ratio of the mortars were 1:2 and 1:3, respectively. The mortars were cast into cylindrical mold (diameter of 100 mm, height of 50 mm). After being cured at 20 ± 1°C and a relative humidity of 90% for 24 h, the sample were demolded and cured in lime saturated water at 20 ± 1°C and >95% relative humidity to testing ages. The rapid chloride migration test method is based on GB/T 50082-2009 and the model diagram is shown in Figure 3. More detailed experimental steps and methods are shown in the Supporting Info. The anode solution was sodium chloride solution with a mass fraction of 10%, the cathode solution was a 0.3 mol/L sodium hydroxide solution, and the

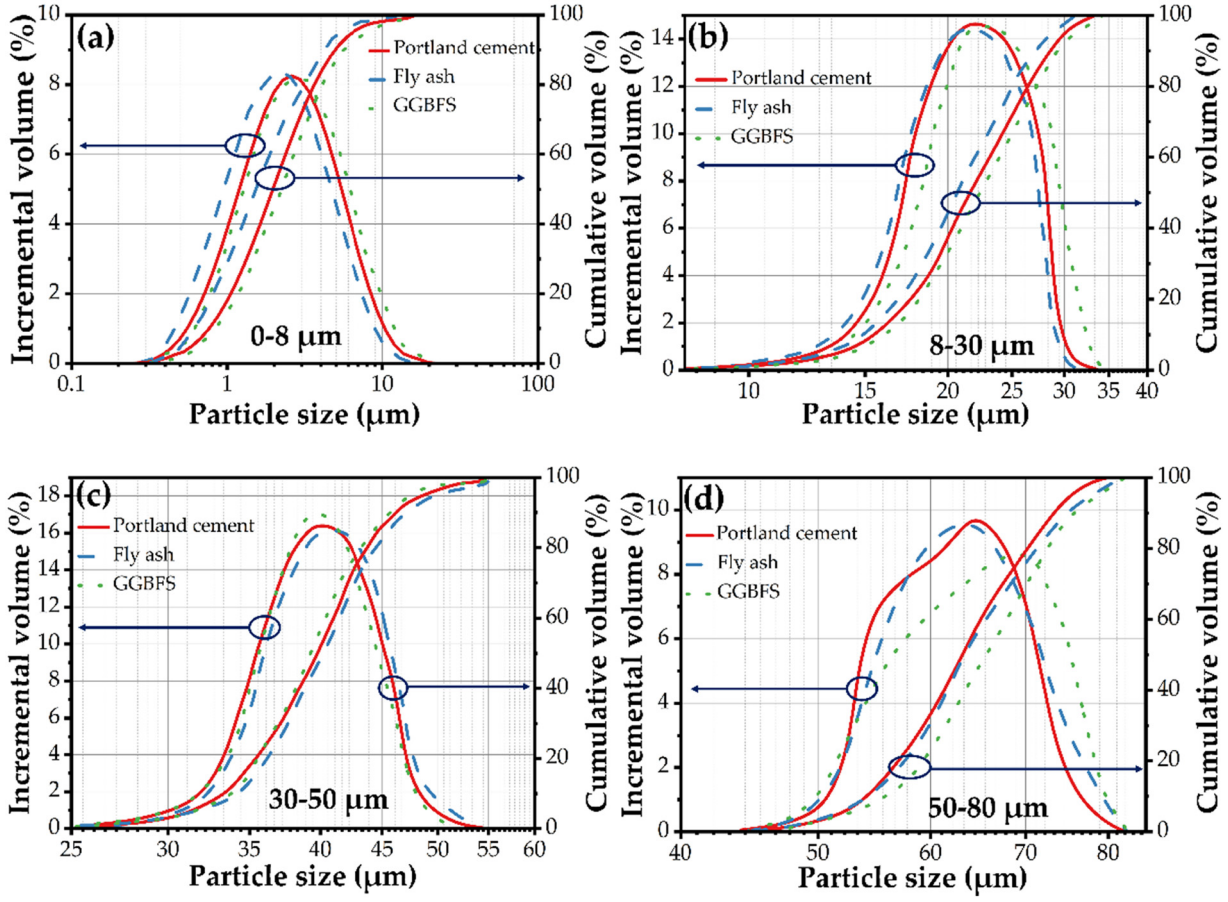

Figure 2: PSD of raw materials in different particle size ranges.

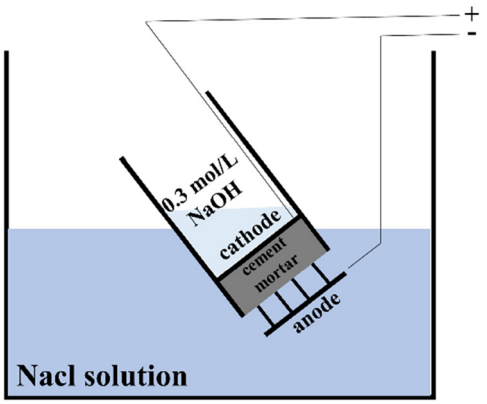

Figure 3: Schematic diagram of rapid chloride migration test.

color indicator was a 0.1 mol/L silver nitrate solution. One specimen was split for the determination of the chloride penetration depth by spraying $AgNO_3$ solution.

2.3 Orthogonal experimental design

To obtain suitable cementitious materials in various particle size ranges, we designed an orthogonal experimental. Orthogonal experimental design is a kind of designing method to study multi-factor and multi-level. According to the orthogonality, some uniformly dispersed and neatly comparable representative points are selected from the comprehensive test [38]. The factors in orthogonal test are the parameters which influence the performance of blended cement pastes, while the level in orthogonal test means the maximum number of the values that can be taken on by any single factor. Consequently, orthogonal experiment was designed to optimize the preparation of blended cement pastes involving multivariate and multi-level factors. To determine the effect of cementitious materials and particle size range on the compressive strength of cement paste, particle sizes of 0–8 μm (A), 8–30 μm (B), 30–50 μm (C), and 50–80 μm (D) were set as four factors in the orthogonal experiment, respectively. The levels of each parameter were determined by selecting some typical values of parameters. Three levels of 0–8, 8–30, 30–50, and 50–80 μm were cement, FA, and GGBFS, respectively. Fuller distribution model was proposed by William B. Fuller and Sanford E. Thomson [39,40], and its mathematical expression is as follows:

$$P(x) = 100 \cdot \left(\frac{x}{D}\right)^n,$$

where $P(x)$ is the cumulative volume of particles through x μm sieve pore (%), x is the size of sieve pore (μm), D is the maximum diameter of particles (μm), n is the distribution index of particles for cement and SCMs. The value of n is generally taken as 0.4. In this study, the value of D can be approximately regarded as 80 μm, and the x (μm) is 8, 30, 50, and 80, respectively. Thus, the cumulative volume of particles through sieve can be calculated by Fuller distribution equation, the result is shown in Table 1. The factors and levels of orthogonal experiment design are shown in Table 2 and the orthogonal experiment design is shown in Table 3.

Table 1: Mixture proportions of blended cements

Fraction (μm)	0–8	8–30	30–50	50–80
Fuller content (%)	39.81	27.74	14.31	17.14
PC			—	

Table 2: Factors and levels of orthogonal experiment design

Levels	Factors			
	A (0–8 μm)	B (8–30 μm)	C (30–50 μm)	D (50–80 μm)
1	Cement	Cement	Cement	Cement
2	FA	FA	FA	FA
3	GGBFS	GGBFS	GGBFS	GGBFS

3 Results and discussion

In this section, the microstructure, hydration products, and chloride ion penetration properties of the blended cements are analyzed and discussed.

3.1 Orthogonal experiment analysis

Nine sets of orthogonal tests were conducted using the experimental method, the test results are shown in Table 4. The results of compressive strength in orthogonal tests were subjected to extreme difference analysis, and the results are presented in Table 5. K_{Xm} is the total value of the experimental results containing the factor X with m level, and k_{Xm} is the mean of the experimental results containing the impact factor X with m level.

According to the results, the optimal ratio for 28-day compressive strength is $A_3B_1C_3D_2$, and the effect degree of the factors on 28-day compressive strength is A > B > C > D. It can be seen that impact factor A (0–8 μm) plays a

Table 3: Orthogonal experiment design

Number	Sample	A	B	C	D	Raw material of each particle size range			
						A (0–8 μm)	B (8–30 μm)	C (30–50 μm)	D (50–80 μm)
1	F-CCCC	1	1	1	1	Cement	Cement	Cement	Cement
2	F-CFFF	1	2	2	2	Cement	FA	FA	FA
3	F-CGGG	1	3	3	3	Cement	GGBFS	GGBFS	GGBFS
4	F-FCFG	2	1	2	3	FA	Cement	FA	GGBFS
5	F-FFGC	2	2	3	1	FA	FA	GGBFS	Cement
6	F-FGCF	2	3	1	2	FA	GGBFS	Cement	FA
7	F-GCGF	3	1	3	2	GGBFS	Cement	GGBFS	FA
8	F-GFCG	3	2	1	3	GGBFS	FA	Cement	GGBFS
9	F-GGFC	3	3	2	1	GGBFS	GGBFS	FA	Cement

Table 4: Results of the orthogonal experiment

Number	1	2	3	4	5	6	7	8	9
28-day compressive strength (MPa)	52.5	27.8	47.7	31.8	24.2	39.8	64.3	52.2	41.5

Table 5: Range analysis on 28-day compressive strength

Factors	28-day compressive strength (MPa)			
	A	B	C	D
K_1	128.0	148.5	136.4	118.1
K_2	95.7	104.2	101.1	131.9
K_3	157.9	128.9	113.3	131.6
k_1	42.7	49.5	45.5	39.4
k_2	31.9	34.7	33.7	44.0
k_3	52.6	43.0	37.8	43.9
R	20.7	14.8	11.8	4.6
Ranking	A > B > C > D			

Note: A: 0–8 μm, B: 8–30 μm, C: 30–50 μm, and D: 50–80 μm.

significant role in 28-day compressive strength, while factor D (50–80 μm) has less influence on 28-day compressive strength and the order of K value for parameter D is D_2, D_3, and D_1. It indicates that the fine particles have a faster hydration reaction rate and higher activity, and therefore their contribution to strength is greater. On the contrary, the reactivity of coarse particles is relatively inert and the rate of hydration reaction is slower, or even no hydration occurs early, which contributes less to the strength of cement paste. Therefore, the optimal proportion of blended cement paste (GGBFS in 0–8 μm, PC in 8–30 μm, GGBFS in 30–50 μm, and FA in 50–80 μm) has a higher 28-day compressive strength, which is labeled as F-GCGF.

3.2 PSD of blended cement

The PSD curves of blended cement based on Fuller model, PC, and reference cement are shown in Figure 4. For the effectiveness of the experiment, we set up an ungraded cementitious material composed of reference cement (27.74% PC + 55.12% GGBFS + 17.14% FA). Reference cement is a blended cement composed of FA, GGBFS, and PC, and the content of each component is consistent with F-GCGF. The results clearly show that the nine groups of samples based on the model were closer to the Fuller curve compared to PC and reference cement.

3.3 Compressive strength

Figure 5 shows the results of compressive strength of blended cement based on the Fuller model, PC, and reference cement pastes. The compressive strength of blended cements based on the Fuller model (F-GCGF) is higher than that of PCs and reference cements at all ages. It indicates that the PSD of F-GCGF promotes strength development. However, the compressive strength of reference cement increased significantly from 7 to 28 days, indicating that the SCMs underwent a secondary hydration reaction with the hydration products during the curing process. F-CCCC has a higher cement clinker content in the nine groups of samples, thus its early strength is superior. However, with the second hydration of SCMs, F-GCGF has the highest strength at 28 days. The samples with higher GGBFS content have higher strength at 28 days, such as F-GFCG, F-GGFC, and F-CGGG. The existence of GGBFS will influence the secondary hydration of C_3A when the mass ratio of GGBFS to cement is above 0.25, and the presence of GGBFS can promote the formation of carboaluminate [41]. The result indicates that the physical filling effect of GGBFS

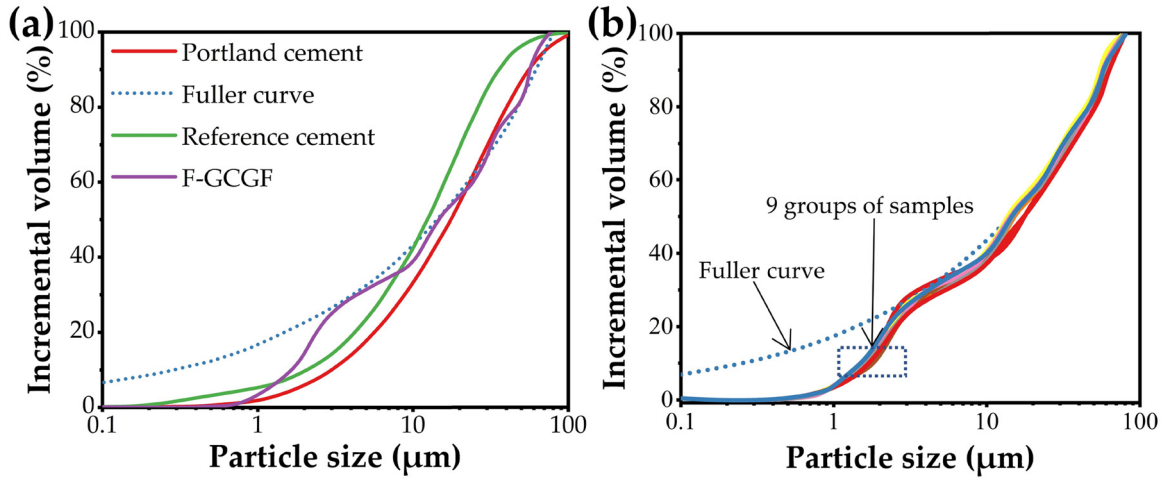

Figure 4: PSD of blended cement based on Fuller model.

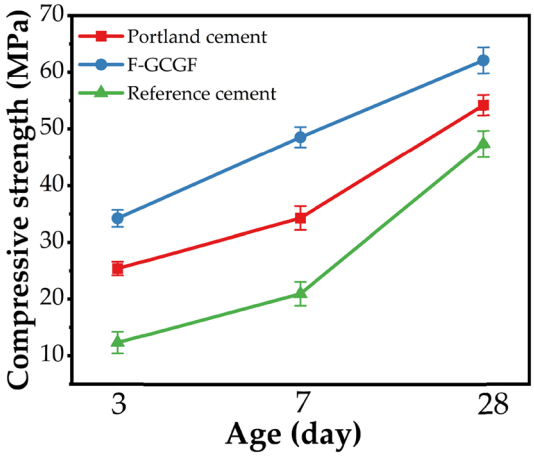

Figure 5: Compressive strength of cement pastes.

particles in 0–8 μm can improve the compactness of the blended cement paste, the dilution and nucleation effect can promote the reaction of blended cement. The cement particles in 8–30 μm provide a major effect on strength without SCMs replacement, and they can be fully hydrated to produce hydration products before 28 days. GGBFS particles in 30–50 μm can provide strength in the later stage through the pozzolanic activity. Whether the cement or FA particles have a small activity within 50–80 μm, the hydration reaction does not occur at an early stage. The present results are in general agreement with the previous studies. High performance blended cements can be prepared by arranging the three components as a high activity SCM, cement clinker, and a low activity SCM in the fine, middle, and coarse fractions, respectively [42].

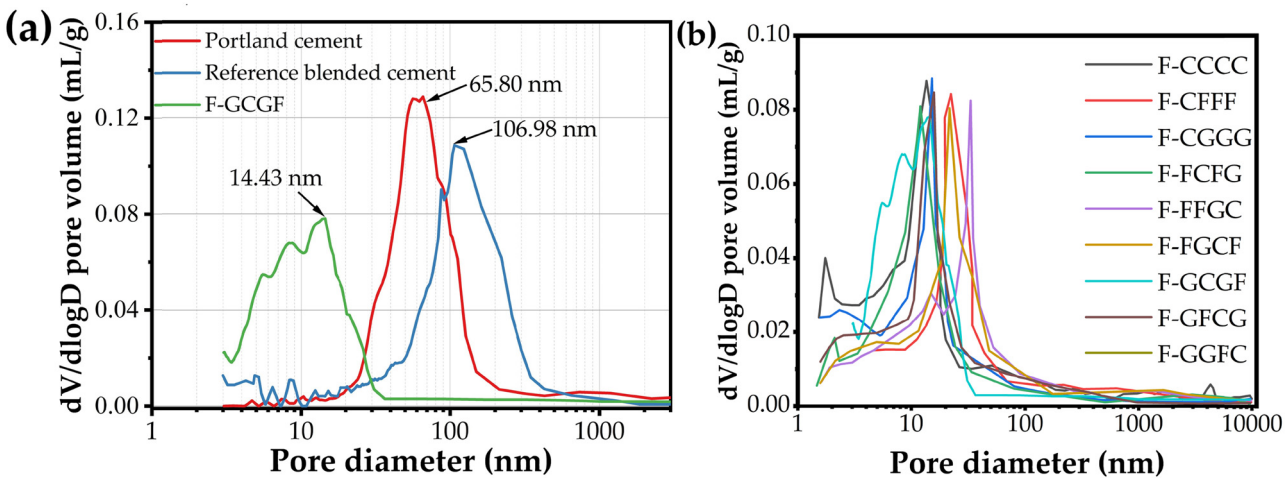

Figure 6: Pore size distribution of blended cement pastes.

3.4 Pore structure

The pore structure of blended cement based on the Fuller model, PC, and reference cement pastes at 28 days is shown in Figure 6. In Figure 6(a), the most probable pore size of reference cement paste is the greatest, followed by PC and the smallest is F-GCGF. According to the influence of different size pores on the strength of cement-based materials, the pores can be divided into four categories: harmless pores (<20 nm), less harmful pores (20–50 nm), harmful pores (50–100 nm), and more harmful pores (>200 nm) [43,44]. It can be presented that there is a large proportion of pores in the reference cement paste, in the form of harmful pores and more harmful pores. Due to the low bonding performance between the particles of SCMs in reference cement paste and the small amount of hydration products, it has an adverse effect on the compressive strength and pore structure of hardened cement paste. In contrast to previous beliefs, F-GCGF has a smaller porosity and a greater proportion of harmless pores with the same water-to-cement ratio. On the one hand, the effect of volcanic ash from ultrafine slag can generate more C–S–H gel, which improves the pore structure of hardened cement [17]. On the other hand, a reasonable particle grading allows the cement paste to achieve a higher initial fill density, thereby reducing harmful pores [21]. In Figure 6(b), the blended cement optimized based on the fuller model has smaller pores, which plays an important role in the improvement of the chloride penetration resistance. The results show that the samples with higher GGBFS content have smaller average pore sizes, which indicates that GGBFS is more susceptible to form a dense structure than FA. It is due to the optimized particle gradation and the volcanic ash reaction of GGBFS, which produces smaller pores and makes the microstructure denser [45].

3.5 Hydration evolution

Figure 7 illustrates the rate of hydration heat evolution and cumulative heat curves of blended cement based on the Fuller model, PC, and reference cement. The hydration

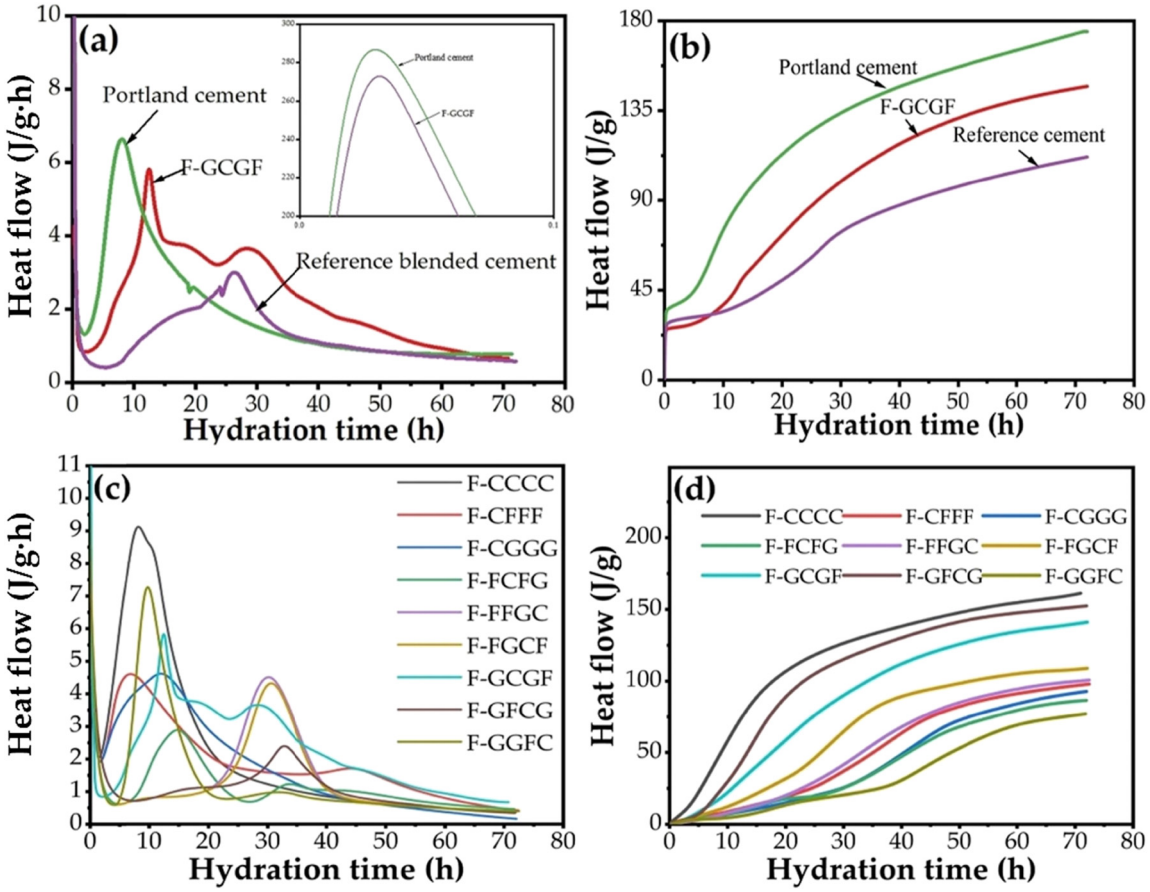

Figure 7: Hydration evolution of blended cement.

heat evolution rate and cumulative heat of reference cement are lower than those of other samples, which is due to the fact that the addition of SCMs can significantly reduce the hydration heat of blended cement. F-GCGF has three exothermic peaks as show in Figure 7(a), which is different from PC and reference cement. For the rate of heat evolution of F-GCGF, the first exothermic peak accrues around 0.03 h and the second peak appears at 10–15 h, which are lower than PC due to the low cement content. The third exothermic peak value (25–35 h) presents quite a high value, which is mainly caused by hydration in 0–8 μm. The results indicate that the activity of the finer GGBFS in the F-GCGF is superior to that of the reference cement. In Figure 7(b), the highest total hydration heat release in 72 h is F-GCGF, and the lowest is reference cement. To sum up, the cumulative hydration heat of F-GCGF for 72 h is only zero point eight times of that of PC, while is about one point four times of that of reference cement. In Figure 7(c and d), F-CCCC has a high cement clinker content and therefore has the highest hydration exotherm. F-FFGC and F-FGCF have a higher secondary hydration degree at about 30 h. The time of the third exothermic peak is not consistent in different samples, which is caused by the different sizes as well as types of cementitious materials [46].

The hydration products and morphology of blended cement pastes after hydration can be seen in Figure 8. Compared to the reference cement, the microstructure of PC and F-GCGF are denser. It demonstrates the high correlation between the compressive strength and the density of the blended cement paste. In order to more accurately identify the mineral phases in each blended cement paste, an energy dispersive spectrometer (EDS) was employed to analyze the composition of cement paste [47–49]. The ratio of elements is essentially the same as the raw material and can be identified as unhydrated particles. At 3 days, the hydration products of PC are the most abundant, with

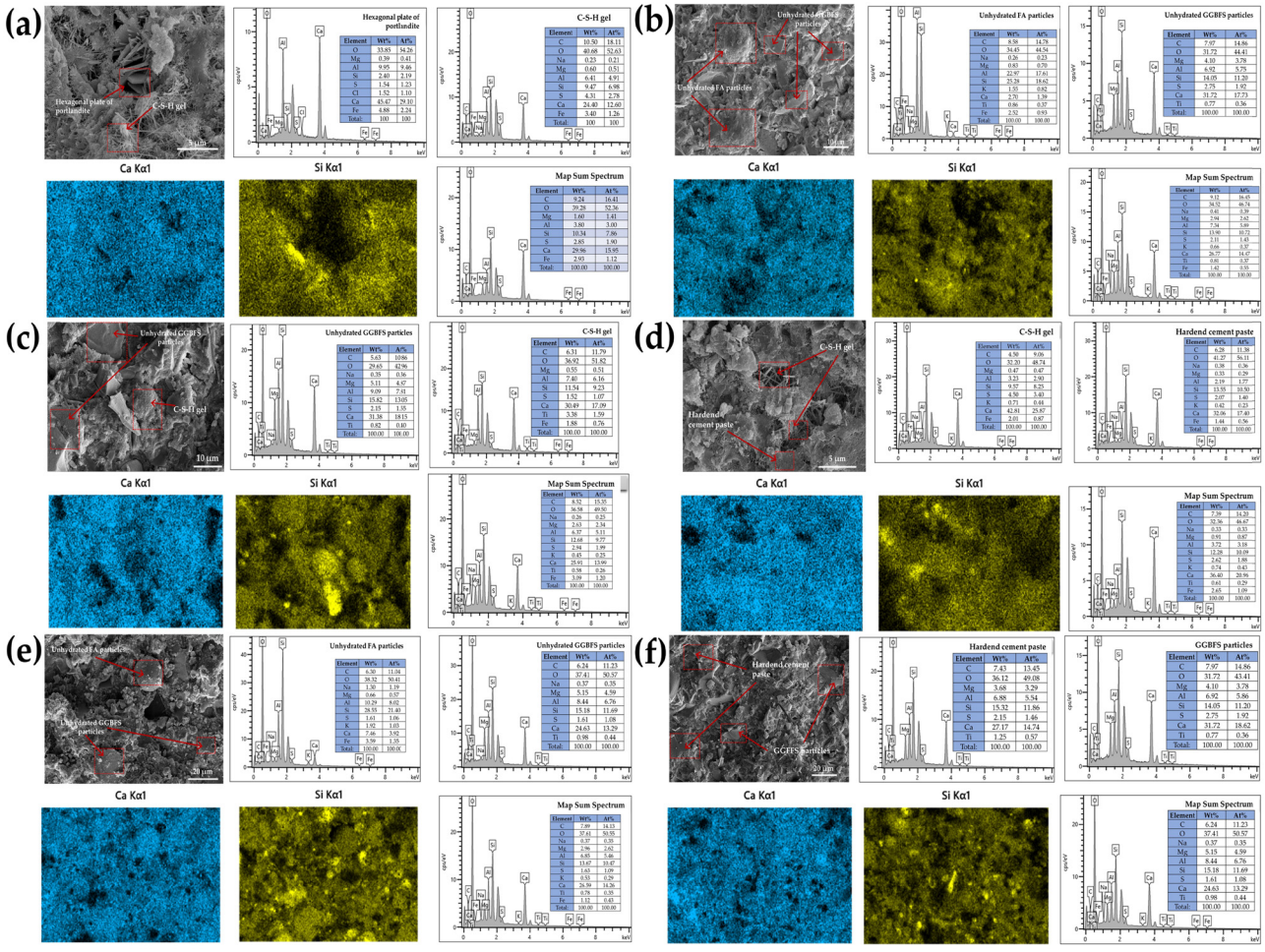

Figure 8: SEM images of blended cement pastes: (a) PC paste cured for 3 days, (b) reference cement paste cured for 3 days, (c) F-GCGF blended cement paste cured for 3 days, (d) PC paste cured for 28 days, (e) reference cement paste cured for 28 days, and (f) F-GCGF-blended cement paste cured for 28 days.

obvious C–S–H gels and hexagonal plates of portlandite. Its calcium to silicon ratio is greater than 2, which is due to its presence of more cement clinker. The presence of significant unhydrated particles in the reference cement, the unhydrated FA particles present a higher proportion of Al and Si, while the unhydrated GGBFS presents a higher proportion of Al, Si, and Ca. The F-GCGF cement paste has more hydration products than the reference cement, and presents a fibrous C–S–H gel on the surface of the GGBFS and FA. Among them, the calcium–silica ratio on the surface of the GGBFS particles in F-GCGF is 1.58, while the calcium–silica ratio of unhydrated GGBFS particles in the reference cement is 1.39, indicating a higher hydration degree in F-GCGF. At 28 days, the results showed that the hydrated calcium silicate filled in the pores of PC, gradually compensated for the structural defects of cementite paste, improved the structure of pores, and enhanced the performance of the samples. Unhydrated FA particles and GGBFS particles are still present in the reference cement withcalcium to silicon ratio of 1.14, which indicates that the particles do not generate C–(A)-S–H gels. In F-GCGF, there are no obvious particles that are not hydrated, and the calcium–silica ratio on the surface of GGBFS particles is 1.66, which shows that they took part in the hydration reaction. The hydrated calcium silicate gels generated by cement clinker and SCMs bond the GGBFS particles together, forming a skeleton and enhancing performance.

It can be seen in the EDS map distribution that the calcium and silicon in the reference cement and F-GCGF are smaller than in PC, which is due to the lower clinker content of the cement and the more uniform distribution of calcium and silicon elements. The EDS map distribution of all elements is shown in Figures S6–S11. The Ca and Si elements were uniformly distributed in all samples, and the brighter regions in the element distribution were those with higher contents of corresponding elements.

The TG–DTA curves of blended cement are shown in Figure 9. It can be seen from Figure 9(a) that there is a mass loss between 100 and 300°C, indicating the dehydration of C–S–H gel, Aft, and AFm phases. A steep mass loss between 400 and 460°C corresponds to the calcium hydroxide decomposition. It was also noted that a small amount of calcium carbonate decarbonate after 600°C due to natural carbonation [50,51]. According to the weight loss of calcium hydroxide at 400°C and calcium carbonate at 500°C, the calcium hydroxide content in the pastes can be calculated. Compared to the calcium hydroxide content of 5.7% in PC, the calcium hydroxide content at 3 days is 2.65 and 2.56% for the F-GCGF and reference blended cement, respectively. Similarly, while the calcium hydroxide content of PC is 8.34%, F-GCGF and reference cement have evidently less calcium hydroxide content of 2.98 and 2.8% at 28 days, respectively.

Due to the abundant of clinker in the PC, it has the highest calcium hydroxide content at 3 and 28 days. It indicates that the addition of SCMs significantly reduces the amount of calcium hydroxide in the pastes under standard curing conditions. The ordinary portland cement (OPC) paste has released more CH content in the initial stage in comparison to OPC with 50% slag [52]. With the increase of curing age, the content of calcium hydroxide in PC pastes is gradually increased due to continuous hydration. On the contrary, the content of calcium hydroxide in F-GCGF and reference cement decreases slightly with increasing age, which is because the pozzolanic effect of GGBFS and FA consumes calcium hydroxide. In previous studies, the composite cement paste had a higher C–S–H gel content and lower calcium hydroxide content compared to the reference cement [53]. Figure 9(b) shows the

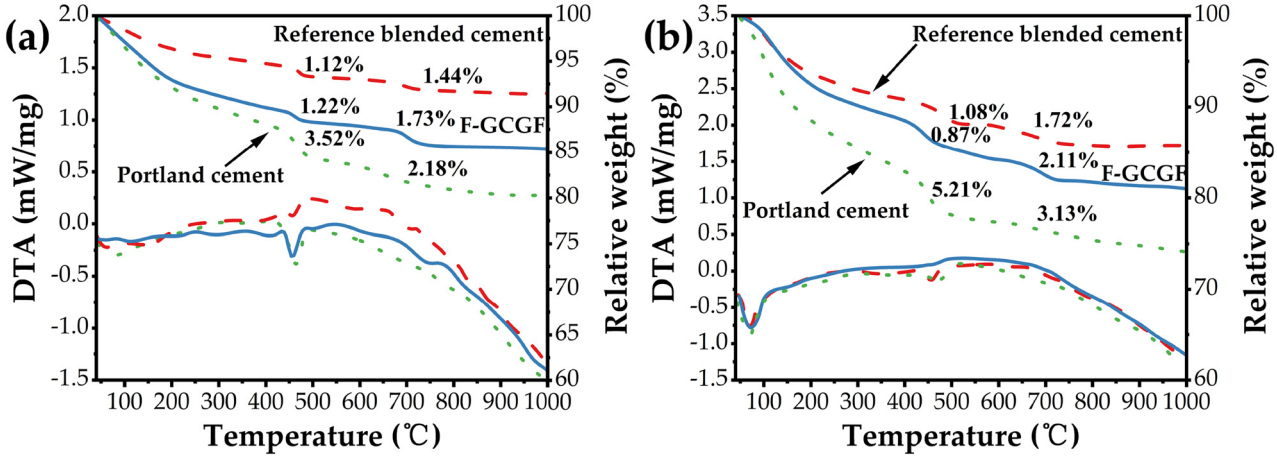

Figure 9: TG–DTA curves of blended cement pastes cured for (a) 3 days and (b) 28 days.

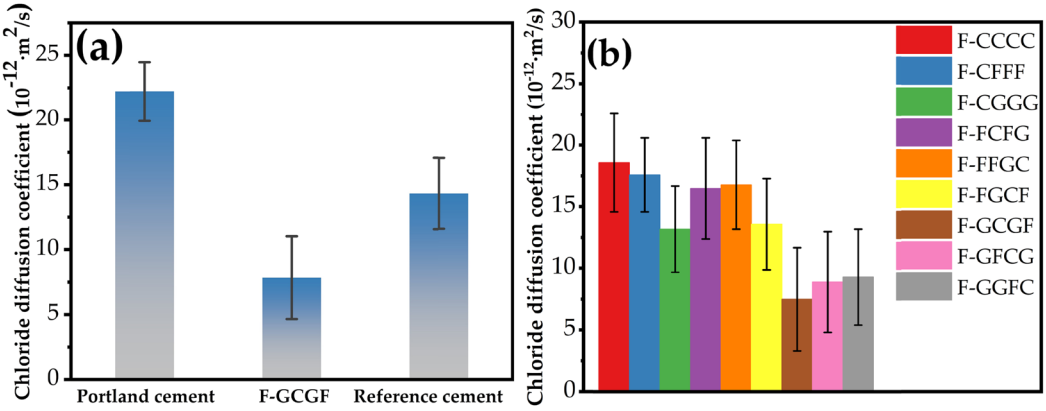

Figure 10: Chloride diffusion coefficient of blended cement mortars.

weight loss of the nine groups of samples at 28 days, with F-CCCC having the highest calcium hydroxide and C–S–H content. And it still shows that the samples with high GGBFS content have more hydration products. It is consistent with previous studies in which the main product was identified as C–S–H. In the pastes with high pH, hydrotalcite was observed at later stages of hydration [54].

3.6 Rapid chloride migration (RCM) test

The chloride diffusion coefficients of the blended cement based on the Fuller model, PC, and reference cement mortars were tested, and results are shown in Figure 10. Figure 10(a) shows that the chloride ion diffusion coefficient in PC mortar is pretty high. In addition, the F-GCGF sample with a reasonable PSD has better chloride ion penetration resistance than the reference cement mortar. It indicates that a reasonable PSD can improve the pore size distribution and porosity in the cement mortar. The profile pictures of each sample sprayed with silver nitrate solution after RCM are shown in Figure S12. Thus, the refinement of the pores prevents the transport of chloride ions, and the blended cement mortar with SCMs has a superior property of chloride ion penetration resistance. The incorporation of ultrafine slag enhances the interfacial transition zone of the cement mortar, and its pozzolanic effect consumes calcium hydroxide in the transition zone [55]. By adding a large amount of SCMs to the cement mortar, the hydration will greatly improve the interface between the aggregates and the paste. From Figure 10(b), it can be concluded that the 28-day compressive strength of the samples is not directly related to the resistance to chloride ion penetration [56]. It is mainly determined by the degree of hydration and particle distribution of SCMs.

4 Conclusions

In this study, the effect of PSD on the microstructure of blended cement with SCMs was examined. The chloride diffusion coefficient of blended cement mortar was also investigated. Based on the results of the orthogonal test, the optimum PSD is GGBFS in 0–8 μm range, PC in 8–30 μm range, GGBFS in 30–50 μm range, and FA in 50–80 μm range. The fine range (0–8 μm) contributed to the greatest strength of the samples. The blended cements based on the Fuller distribution model have less porosity and a denser micromorphology, which is due to their reasonable PSD and the volcanic ash reaction of SCMs. At 28 days, the filling and hydration effect of GGBFS is superior, which makes the blended cement paste structure denser. The hydration exothermic results confirm that the higher the cement clinker content, the higher the hydration degree of the samples. The delayed onset of the third exothermic peak in samples containing SCMs indicates volcanic ash effect, especially in samples with high GGBFS content. The TG–DTA curves indicate that the volcanic ash effect of GGBFS and FA leads to a reduction in the calcium hydroxide content of the reference cement and F-GCGF. Due to the filling effect and volcanic ash effect of ultrafine in blended cement mortar, its physical adsorption and chemical bonding abilities are enhanced. The compressive strength and the resistance to chloride ion penetration are not directly related, but depend more on the particle distribution of the blended cement and the hydration degree of the SCMs. The present work only enhances the chloride permeability in cement mortars. Furthermore, the PSD of other SCMs can be investigated in future work, such as improving the freeze–thaw resistance of concrete.

Funding information: This research was funded by the Key Program of the National Natural Science Foundation of

China (grant number: 51732008) and the National Key Research and Development Program of China (grant numbers: 2019YFC1520500 and 2019YFC1520104).

Conflict of interest: Authors state no conflict of interest.

Data availability statement: The raw/processed data required to reproduce these findings cannot be shared at this time as the data also forms part of ongoing study.

References

[1] Zhang N, Tang B, Liu X. Cementitious activity of iron ore tailing and its utilization in cementitious materials, bricks and concrete. Constr Build Mater. 2021;288:123022.
[2] Qaidi S, Najm HM, Abed SM, Ahmed HU, Al Dughaishi H, Al Lawati J, et al. Fly ash-based geopolymer composites: a review of the compressive strength and microstructure analysis. Materials. 2022;15:7098.
[3] Ramezanianpour AM, Hooton RD. Sulfate resistance of Portland-limestone cements in combination with supplementary cementitious materials. Mater Struct. 2013;46:1061–73.
[4] Gettu R, Patel A, Rathi V, Prakasan S, Basavaraj AS, Palaniappan S, et al. Influence of supplementary cementitious materials on the sustainability parameters of cements and concretes in the Indian context. Mater Struct. 2019;52:1–11.
[5] Etim MA, Babaremu K, Lazarus J, Omole D. Health risk and environmental assessment of cement production in Nigeria. Atmosphere. 2021;12:1111.
[6] Zhao Y, Yu M, Xiang Y, Kong F, Li L. A sustainability comparison between green concretes and traditional concrete using an emergy ternary diagram. J Clean Prod. 2020;256:120421.
[7] Aïtcin PC. High-performance concrete. London: Taylor and Francis; 2004.
[8] Miller SA. Supplementary cementitious materials to mitigate greenhouse gas emissions from concrete: can there be too much of a good thing. J Clean Prod. 2018;178:587–98.
[9] Chen JJ, Kwan AKH. Superfine cement for improving packing density, rheology and strength of cement paste. Cem Concr Compos. 2012;34:1–10.
[10] Ghafari E, Ghahari S, Feys D, Khayat K, Baig A, Ferron R. Admixture compatibility with natural supplementary cementitious materials. Cem Concr Compos. 2020;112:103683.
[11] Saha AK. Effect of class F fly ash on the durability properties of concrete. Sustain Environ Res. 2018;28:25–31.
[12] Liu Z, Ni W, Li Y, Ba H, Li N, Ju Y, et al. The mechanism of hydration reaction of granulated blast furnace slag-steel slag-refining slag-desulfurization gypsum-based clinker-free cementitious materials. J Build Eng. 2021;44:103289.
[13] Arafa S, Milad A, Yusoff NIM, Al-Ansari N, Yaseen ZM. Investigation into the permeability and strength of pervious geopolymer concrete containing coated biomass aggregate material. J Mater Res Technol. 2021;15:2075–87.
[14] Haustein E, Kuryłowicz-Cudowska A, Łuczkiewicz A, Fudala-Książek S, Cieślik BM. Influence of cement replacement with sewage sludge ash (SSA) on the heat of hydration of cement mortar. Materials. 2022;15:1547.
[15] Kawabata Y, Yamada K. The mechanism of limited inhibition by fly ash on expansion due to alkali–silica reaction at the pessimum proportion. Cem Concr Res. 2017;92:1–15.
[16] Nili M, Ehsani A. Investigating the effect of the cement paste and transition zone on strength development of concrete con-taining nanosilica and silica fume. Mater Des. 2015;75:174–83.
[17] Ahmad J, Kontoleon KJ, Majdi A, Naqash MT, Deifalla AF, Ben Kahla N, et al. A comprehensive review on the ground granulated blast furnace slag (GGBS) in concrete production. Sustainability. 2022;14:8783.
[18] Siline M. Efficiency of incorporating Algerian ground granulated blast furnace slag as a supplementary cementitious material: a review. Innov Infrastruct Solut. 2022;7:121.
[19] Bentz DP, Hansen AS, Guynn JM. Optimization of cement and fly ash particle sizes to produce sustainable concretes. Cem Concr Compos. 2011;33:824–31.
[20] Syvitski JPM. Principles, methods and application of particle size analysis. Cambridge: Cambridge University Press; 1991.
[21] Elaqra H, Rustom R. Effect of using glass powder as cement replacement on rheological and mechanical properties of cement paste. Constr Build Mater. 2018;179:326–35.
[22] Qin R, Zhou A, Yu Z, Wang Q, Lau D. Role of carbon nanotube in reinforcing cementitious materials: an experimental and coarse-grained molecular dynamics study. Cem Concr Res. 2021;147:106517.
[23] Jiao D, Shi C, Yuan Q, An X, Liu Y, Li H. Effect of constituents on rheological properties of fresh concrete – a review. Cem Concr Res. 2017;83:146–59.
[24] Sun X, Zhao Y, Tian Y, Wu P, Guo Z, Qiu J, et al. Modification of high-volume fly ash cement with metakaolin for its utilization in cemented paste backfill: the effects of metakaolin content and particle size. Powder Technol. 2021;393:539–49.
[25] Wang J, Liu M, Wang Y, Zhou Z, Xu D, Du P, et al. Synergistic effects of nano-silica and fly ash on properties of cement-based composite. Constr Build Mater. 2020;262:120737.
[26] Ebailila M, Kinuthia J, Oti J, Al-Waked Q. Sulfate soil stabilisation with binary blends of lime–silica fume and lime–ground granulated blast furnace slag. Transp Geotech. 2022;37:100888.
[27] Wang Y, He X, Su Y, Tan H, Yang J, Lan M, et al. Self-hydration characteristics of ground granulated blast-furnace slag (GGBFS) by wet-grinding treatment. Constr Build Mater. 2018;167:96–105.
[28] Li T, Lin J, Liu J. Analysis of time-dependent seismic fragility of the offshore bridge under the action of scour and chloride ion corrosion. Structures. 2020;28:1785–801.
[29] Tian Y, Zhang G, Ye H, Zeng Q, Zhang Z, Tian Z, et al. Corrosion of steel rebar in concrete induced by chloride ions under natural environments. Constr Build Mater. 2023;369:130504.
[30] Mehta P, Monteiro P. Concrete: microstructure, properties, and materials. 3rd edn. New York: McGraw-Hill Professional; 2013.
[31] Juenger MCG, Siddique R. Recent advances in understanding the role of supplementary cementitious materials in concrete. Cem Concr Compos. 2015;78:71–80.
[32] Zhang T, Yu Q, Wei J, Gao P, Chen P, Hu J. Micro-structural development of gap-graded blended cement pastes containing a high amount of supplementary cementitious materials. Cem Concr Compos. 2012;34:1024–32.

[33] Lee NK, Lee HK. Influence of the slag content on the chloride and sulfuric acid resistances of alkali-activated fly ash/slag paste. Cem Concr Compos. 2016;72:168–79.
[34] Chen X, He Y, Lu L, Wang F, Hu S. Effects of curing regimes on the chloride binding capacity of cementitious materials. Constr Build Mater. 2022;342:127929.
[35] Zhang T, Gao P, Luo R, Guo Y, Wei J, Yu Q. Measurement of chemical shrinkage of cement paste: comparison study of ASTM C 1608 and an improved method. Constr Build Mater. 2013;48:662–9.
[36] EN 196-1. Methods of testing cement: determination of strength. London: British Standards Institution; 2005.
[37] ASTM C 1702-09A. Standard test method for measurement of heat of hydration of hydraulic cementitious materials using isothermal conduction calorimetry. New York: American Society for Testing and Materials; 2009.
[38] Li XJ, Hao JY. Orthogonal test design for optimization of synthesis of super early strength anchoring material. Constr Build Mater. 2018;181:42–8.
[39] Gong C, Zhang J, Wang S, Lu L. Effect of aggregate gradation with fuller distribution on properties of sulphoaluminate cement concrete. J Wuhan Univ Technol. 2015;30:1029–35.
[40] Zhao J, Wang D, Yan P. Design and experimental study of a ternary blended cement containing high volume steel slag and blast-furnace slag based on Fuller distribution model. Constr Build Mater. 2017;140:248–56.
[41] Nie R, Wu Q, Yu Z, Wang A, Shen X. Effect of coral powder and ground-granulated blast-furnace slag on the hydration behavior of cement paste. J Therm Anal Calorim. 2022;147:6643–54.
[42] Zhang T, Yu Q, Wei J, Zhang P. A new gap-graded particle size distribution and resulting consequences on properties of blended cement. Cem Concr Compos. 2011;33:543–50.
[43] Ying J, Zhou B, Xiao J. Pore structure and chloride diffusivity of recycled aggregate concrete with nano-SiO_2, and nano-TiO_2. Constr Build Mater. 2017;150:49–55.
[44] Allen AJ, Thomas JJ, Jennings HM. Composition and density of nanoscale calcium-silicate-hydrate in cement. Nat Mater. 2017;6:311–6.
[45] Yao G, Wang Q, Su Y, Wang J, Qiu J, Lyu X. Mechanical activation as an innovative approach for the preparation of pozzolan from iron ore tailings. Min Eng. 2020;145:106068.
[46] Zhang T, Yu Q, Wei J, Zhang P. Efficient utilization of cementitious materials to produce sustainable blended cement. Cem Concr Compos. 2012;34:692–9.
[47] Zunino F, Scrivener K. The influence of sulfate addition on hydration kinetics and C–S–H morphology of C_3S and C_3S/C_3A systems. Cem Concr Res. 2022;160:106930.
[48] Fu Q, Zhang Z, Zhao X, Xu W, Niu D. Effect of nano calcium carbonate on hydration characteristics and microstructure of cement-based mateials: a review. J Build Eng. 2022;50:104220.
[49] Shui Z, Zhang R, Chen W, Xuan D. Effects of mineral admixtures on the thermal expansion properties of hardened cement paste. Constr Build Mater. 2010;24:1761–7.
[50] Zhang MH, Li H. Pore structure and chloride permeability of concrete containing nano-particles for pavement. Constr Build Mater. 2011;25:608–16.
[51] Tsivilis S, Kakali G, Chaniotakis E, Souvaridou A. A study on the hydration of Portland limestone cement by means of TG. J Therm Anal Calorim. 1998;52:863–70.
[52] Zhang Q, Zhang B, Feng Y, Qi C, Chen Q, Xiao C. Hydration development of blended cement paste with granulated copper slag modified with CaO and Al_2O_3. J Mater Res Technol. 2022;18:909–20.
[53] Zhang T, Yu Q, Wei J, Li J, Zhang P. Preparation of high performance blended cement and reclamation of iron concentrate from basic oxygen furnace steel slag. Resour Conserv Recycl. 2011;56:48–55.
[54] Song S, Sohn D, Jennings HM, Mason TO. Hydration of alkali-activated ground granulated blast furnace slag. J Mater Sci Technol. 2000;35:249–57.
[55] Li X, Zhang Q. Influence behavior of phosphorus slag and fly ash on the interface transition zone in concrete prepared by cement-red mud. J Build Eng. 2022;49:104017.
[56] Sim J, Park C. Compressive strength and resistance to chloride ion penetration and carbonation of recycled aggregate concrete with varying amount of fly ash and fine recycled aggregate. Waste Manage. 2011;31:2352–60.